Nuclear Engineering and Design 239 (2009) 1314–1322

Contents lists available at ScienceDirect

Nuclear Engineering and Design

journal homepage: www.elsevier.com/locate/nucengdes

k–ε modeling using modified nodal integral method

Suneet Singh*, Rizwan-uddin

Department of Nuclear Plasma and Radiological Engineering, University of Illinois at Urbana-Champaign, 216 Talbot Lab, 104 S. Wright St., Urbana, IL 61801, United States

ARTICLE INFO

Article history:
Received 7 September 2008
Received in revised form 4 March 2009
Accepted 10 March 2009

ABSTRACT

The simulation of turbulent flows is an ongoing challenge. This is especially true for the flows in the nuclear reactors. In order to save computational time and resource, accurate numerical schemes are required for such simulations. The encouraging results from the laminar flow simulations using modified nodal integral method (MNIM), serves as a motivation to use the method for turbulent flow simulations. The k–ε model in this work has been implemented using the MNIM formulation. Two models, one for low Reynolds number and one for high Reynolds number, are implemented. The application of the model to relatively simple problems shows that results are good and similar to what one would expect from the k–ε model implementation with any other numerical scheme. The results are compared with the DNS data from various sources in the literature. The difference between the DNS data and current implementation arises mainly from the assumption made in the k–ε model rather than the choice of the numerical scheme in the present work. It is seen that very coarse grids can be used away from the walls for the present simulation. This is especially true for low Reynolds number model. Hence, MNIM formulation for the k–ε model promises to reduce the over all computational cost.

1. Introduction

Nodal methods, first developed for multi-group neutron diffusion and neutron transport equations, now constitute the backbone of production codes used in the nuclear industry. An early review of nodal methods, developed and used by the nuclear industry, is given by Lawrence (1986). Nodal schemes are developed by approximately satisfying the governing differential equations on finite size brick-like elements that are obtained by discretizing the space of independent variables.

Similar approaches have been used in other branches of science and engineering to develop efficient numerical schemes (Wescott and Rizwan-uddin, 2001; Horak and Dorning, 1985; Elnawawy et al., 1990). Nodal methods, as a general class of computational schemes, are discussed by Hennart (1986). Nodal integral methods (NIM), a subclass of nodal methods, have been developed for the steady-state (Azmy and Dorning, 1983) and time-dependent (Wilson et al., 1988) Navier–Stokes equations. NIM was applied to the steady-state Boussinesq equations for natural convection, and to several steady-state incompressible flow problems (Azmy, 1985). Esser and Witt (1993) developed a nodal scheme for the two-dimensional, vorticity-stream function formulation of the Navier–Stokes equations. This development – that leads to inherent upwinding in the numerical scheme – however cannot be easily extended to three dimensions. NIM was also developed and applied to the time-dependent heat conduction problem (Wilson et al., 1988). Michael et al. (2001) developed a second- and a third-order NIM for the convection–diffusion equation.

Though highly innovative, those early applications of nodal methods for the Navier–Stokes equations did not take full advantage of the potential that the nodal approach offers. An improved method has recently been developed to solve the incompressible Navier–Stokes equations. This modified nodal integral method (MNIM) was first developed for 2D, time-dependent problems (Wang and Rizwan-uddin, 2003) and then extended for 3D, time-dependent flows as well (Wang and Rizwan-uddin, 2005).

The k–ε model, a two equation model, is the most commonly used model for the simulation of the turbulent flows (Durbin and Reif, 2001). The widespread use of this model can be attributed to the fact that it produces *reasonably* good results with relatively less computational effort. Several variations of these models are developed and implemented in the last four decades. Although this model has several limitations, relatively much more extensive computational requirements for alternative models and approaches make the k–ε based approaches fairly popular. It is expected that it will remain the method of choice in the near future. This is especially true for complex engineering flows.

The k–ε model implementation is carried out by incorporating eddy viscosity in the recently developed MNIM for incompressible Navier–Stokes equations. The NIM solver for k and ε equations are also developed and incorporated into a computer code. The flow

* Corresponding author.
E-mail addresses: suneet.singh@gmail.com (S. Singh), rizwan@uiuc.edu (Rizwan-uddin).

0029-5493/$ – see front matter © 2009 Elsevier B.V. All rights reserved.
doi:10.1016/j.nucengdes.2009.03.006

simulations for some simple flows are carried out to verify the computer code.

2. Review of MNIM

A brief description of the NIM as applied to a generic 3D convection–diffusion equation is presented here. The NIM illustrated here for a generic convection–diffusion equation has been used later as a basis for developing numerical schemes for the k and ε equations. Focus here is to identify the unique set of discrete equations that result in a nodal scheme. Details of the scheme are given by Wang and Rizwan-uddin (2003) and Wang and Rizwan-uddin (2005).

The space time domain (X, Y, Z, T) is discretized in parallelepiped cells (i, j, k, n) of size $(2a_i \times 2b_j \times 2c_k \times 2\tau_n)$ with cell centered local coordinates $(x, y, z, t; -a_i \le x \le a_i, -b_j \le y \le b_j, -c_k \le z \le c_k, -\tau_n \le t \le \tau_n)$. The convection–diffusion equation in a cell is written as follows:

$$\frac{\partial C(x,y,z,t)}{\partial t} + u(x,y,z,t)\frac{\partial C(x,y,z,t)}{\partial x} + v(x,y,z,t)\frac{\partial C(x,y,z,t)}{\partial y} + w(x,y,z,t)\frac{\partial C(x,y,z,t)}{\partial z} = \bar{D}\left(\frac{\partial^2 C(x,y,z,t)}{\partial x^2} + \frac{\partial^2 C(x,y,z,t)}{\partial y^2} + \frac{\partial^2 C(x,y,z,t)}{\partial z^2}\right) + s(x,y,z,t) \quad (1)$$

In the above equation, C is a physical quantity (e.g. k or ε) undergoing convection and diffusion in the flow field given by velocity components u, v and w in the x, y and z, directions, respectively.

The next step in the NIM is the transverse integration procedure (TIP). The TIP involves local averaging of the PDE over the cell in all independent variables except one, which results in a corresponding ODE. This process is repeated for all independent variables yielding three transverse integrated ODEs in the space variables, and one ODE in time. For example, averaging over y, z and t i.e. operating by $\frac{1}{8b_jc_k\tau_n}\int_{-\tau_n}^{+\tau}\int_{-b_j}^{+b_j}\int_{-c_k}^{+c_k} dydzdt$, one gets,

$$\bar{D}\frac{d^2\bar{C}^{yzt}(x)}{dx^2} - \bar{u}\frac{d\bar{C}^{yzt}(x)}{dx} = \bar{S}^{yzt}(x) \quad (2)$$

where, $\bar{u}$, $\bar{v}$ and $\bar{w}$ are cell averaged velocity components,

$$\bar{C}^{yzt}(x) \equiv \frac{1}{8b_jc_k\tau_n}\int_{-\tau_n}^{+\tau}\int_{-b_j}^{+b_j}\int_{-c_k}^{+c_k} C(x,y,z,t)dydzdt \quad (3)$$

and the pseudo-source term $\bar{S}^{yzt}(x)$ is defined as

$$\bar{S}^{yzt}(x) \equiv \frac{1}{8b_jc_k\tau_n}\int_{-\tau_n}^{+\tau}\int_{-b_j}^{+b_j}\int_{-c_k}^{+c_k}\left(\bar{D}\left(-\frac{\partial^2 C}{\partial y^2} - \frac{\partial^2 C}{\partial z^2}\right) - s(x,y,z,t) + \bar{v}\frac{\partial C}{\partial y} + \bar{w}\frac{\partial C}{\partial z} + \frac{\partial C}{\partial t}\right)dydzdt \quad (4)$$

To average the convection term, $u(\partial C/\partial x)$, average of the product is approximated by the product of the averages which is known to be a second-order approximation.

The ODEs are solved after pseudo-source terms are expanded and truncated at a desired order. A set of discrete equations for surface-averaged variables is obtained in terms of truncated pseudo-source terms by imposing continuity of C and its corresponding flux (for second-order ODEs) at interfaces, for example, at the interface between cell (i, j, k, n) and $(i+1, j, k, n)$. Similar steps when applied to the ODE in time results in a scheme for marching in time.

In the final step, the truncated pseudo-source terms are eliminated by imposing certain constraints. The constraint equations are obtained by satisfying the PDE over a cell in an average sense and imposing the condition that cell averaged variables be unique, i.e. independent of the order of integration.

The NIM procedure as discussed above after a lot of algebra carried out using Mathematica® yields the following set of discrete equations,

$$F_{57}\bar{C}^{yzt}_{i,j,k,n} - F_{51}\bar{C}^{yzt}_{i-1,j,k,n} - F_{52}\bar{C}^{yzt}_{i+1,j,k,n} = F_{53}(\bar{C}^{xyz}_{i,j,k,n} + \bar{C}^{xyz}_{i,j,k,n-1}) + F_{54}(\bar{C}^{xyz}_{i+1,j,k,n} + \bar{C}^{xyz}_{i+1,j,k,n-1}) \quad (5)$$

$$F_{67}\bar{C}^{zxt}_{i,j,k,n} - F_{61}\bar{C}^{zxt}_{i,j-1,k,n} - F_{62}\bar{C}^{zxt}_{i,j+1,k,n} = F_{63}(\bar{C}^{xyz}_{i,j,k,n} + \bar{C}^{xyz}_{i,j,k,n-1}) + F_{64}(\bar{C}^{xyz}_{i,j+1,k,n} + \bar{C}^{xyz}_{i,j+1,k,n-1}) \quad (6)$$

$$F_{47}\bar{C}^{xyt}_{i,j,k,n} - F_{41}\bar{C}^{xyt}_{i,j,k-1,n} - F_{42}\bar{C}^{xyt}_{i,j,k+1,n} = F_{43}(\bar{C}^{xyz}_{i,j,k,n} + \bar{C}^{xyz}_{i,j,k,n-1}) + F_{44}(\bar{C}^{xyz}_{i,j,k+1,n} + \bar{C}^{xyz}_{i,j,k+1,n-1}) \quad (7)$$

$$F_{77}\bar{C}^{xyz}_{i,j,k,n} - F_{78}\bar{C}^{xyz}_{i,j,k,n-1} = f + F_{71}\bar{C}^{xyt}_{i,j,k,n} + F_{72}\bar{C}^{xyt}_{i,j,k-1,n} + F_{73}\bar{C}^{yzt}_{i,j,k,n} + F_{74}\bar{C}^{yzt}_{i-1,j,k,n} + F_{75}\bar{C}^{zxt}_{i,j,k,n} + F_{76}\bar{C}^{zxt}_{i,j-1,k,n} + F_{78}\bar{C}^{xyz}_{i,j,k,n-1} \quad (8)$$

In the above equations $\bar{C}^{yzt}_{i-1,j,k,n} \equiv \bar{C}^{yzt}_{i,j,k,n}(x = -a_i)$ and $\bar{C}^{yzt}_{i,j,k,n} \equiv \bar{C}^{yzt}_{i,j,k,n}(x = +a_i)$, etc. are used. In the above equations, the subscripts i, j, k and n in the coefficients F and in f are omitted for the sake of clarity. (The subscripts on F may seem strange. These are however the last set of coefficients in a string of coefficients defined and used in the development of the final set of equations. The detailed derivation of these coefficients for the Navier–Stokes equation can be found in Wang and Rizwan-uddin (2003) and Wang and Rizwan-uddin (2005).) The other coefficients were successfully eliminated in favor of this final set.

Also, the coefficient f in the equation is the source term averaged over the node i.e.,

$$f_{i,j,k,n} = \frac{1}{16a_ib_jc_k\tau_n}\int_{-\tau_n}^{\tau_n}\int_{-c_k}^{+c_k}\int_{-b_j}^{+b_j}\int_{-a_i}^{+a_i} s(x,y,z,t)dxdydzdt \quad (9)$$

Development of the MNIM for the momentum equations is similar to that for the convection–diffusion equation. Explicitly, the u-momentum equation in a cell is written as

$$\frac{\partial u(x,y,z,t)}{\partial t} + \bar{u}_p\frac{\partial u(x,y,z,t)}{\partial x} + \bar{v}_p\frac{\partial u(x,y,z,t)}{\partial y} + \bar{w}_p\frac{\partial u(x,y,z,t)}{\partial z} = \nu\left(\frac{\partial^2 u(x,y,z,t)}{\partial x^2} + \frac{\partial^2 u(x,y,z,t)}{\partial y^2} + \frac{\partial^2 u(x,y,z,t)}{\partial z^2}\right) + s(x,y,z,t) \quad (10)$$

where the source term s is defined as follows:

$$s(x,y,z,t) \equiv -\frac{1}{\rho}\frac{\partial p}{\partial x} + (\bar{u}_0 - \bar{u}_p)\frac{\partial u}{\partial x} + (\bar{v}_0 - \bar{v}_p)\frac{\partial u}{\partial y} + (\bar{w}_0 - \bar{w}_p)\frac{\partial u}{\partial z} + g_x \quad (11)$$

and $\bar{u}_0$, $\bar{v}_0$, $\bar{w}_0$ and $\bar{u}_p$, $\bar{v}_p$, $\bar{w}_p$ cell averaged velocity components at current time step and previous time step respectively. In the above equations ν is kinematic viscosity, p is pressure, ρ is density and g_x is the body force term in the x-direction. The discretized equations are same as that of convection diffusion equation except that the f term needs to be suitably modified because the source term, $s(x, y,$

z, t), in this equation is modified as shown in Eq. (11). In evaluating the f term for the Navier–Stokes equation average of the products is approximated by the product of the averages (Wang and Rizwan-uddin, 2003).

The pressure equation is not discussed here as it remains same as in the laminar flow. The details of the numerical scheme for the pressure are given by Wang and Rizwan-uddin (2003).

3. k–ε model

The following are the equations for the k–ε model. These equations are written in the tensor form and Einstein's summation convention (the indices for the equation are m and p) is valid for these equations.

Reynolds averaged Navier–Stokes equation:

$$\frac{\partial \bar{u}_m}{\partial t} + \bar{u}_p \frac{\partial \bar{u}_m}{\partial x_p} = -\frac{1}{\rho}\frac{\partial p}{\partial x_m} + \frac{\partial}{\partial x_p}\left((\nu + \nu_t)\frac{\partial \bar{u}_m}{\partial x_p}\right) + g_m. \tag{12}$$

In the above equation $\bar{u}_m$ and g_m is the Reynolds averaged velocity component in mth direction.

Transport equation for turbulent kinetic energy (k)

$$\frac{\partial k}{\partial t} + \bar{u}_p \frac{\partial k}{\partial x_p} = \frac{\partial}{\partial x_p}\left(\nu + \frac{\nu_t}{\sigma_k}\right)\frac{\partial k}{\partial x_p} + 2\nu_t \bar{s}_{mp}\bar{s}_{mp} - \varepsilon \tag{13}$$

where,

$$\bar{s}_{mp} = \left(\frac{\partial \bar{u}_m}{\partial x_p} + \frac{\partial \bar{u}_p}{\partial x_m}\right). \tag{14}$$

and equation for dissipation of turbulent kinetic energy ($\boldsymbol{\varepsilon}$):

$$\frac{\partial \varepsilon}{\partial t} + \bar{u}_p \frac{\partial \varepsilon}{\partial x_p} = \frac{\partial}{\partial x_p}\left(\nu + \frac{\nu_t}{\sigma_\varepsilon}\right)\frac{\partial \varepsilon}{\partial x_p} + 2C_{1\varepsilon}\frac{\varepsilon}{k}\nu_t \bar{s}_{mp}\bar{s}_{mp} - C_{2\varepsilon}\frac{\varepsilon^2}{k}. \tag{15}$$

The eddy viscosity (ν_t) in the above equations is evaluated as

$$\nu_t = C_\mu \frac{k^2}{\varepsilon}. \tag{16}$$

In the above equations, $C_{1\varepsilon}$, $C_{2\varepsilon}$, C_μ, σ_k, and σ_ε are model constants. The values of these constants vary based on the specific variation of the model used. The model constants for standard k–ε model are given in Table 1 (Durbin and Reif, 2001).

The details of this model (and some of its slightly modified variations) can be found in standard textbooks dealing with turbulence modeling (e.g. Durbin and Reif, 2001).

4. Near wall k–ε modeling

The modeling approach given in the previous section is not valid in the regions near the walls because the model constants are not calibrated for these regions. Moreover, flow becomes laminar in the vicinity of the wall and therefore, eddy viscosity should go to zero as one approaches the wall. Several approaches have been developed to overcome this limitation of the k–ε model. These approaches are broadly classified as: (a) low Reynolds number models; and (b) high Reynolds number models. A low Reynolds number model, as the name suggests, is valid for the flows with relatively low Reynolds number. In these flows the effect of the wall is present in the regions which are significantly away from the wall. However, for the high Reynolds number flows the effect of the wall is present only in the immediate vicinity of the wall, hence the need for a different modeling strategy.

4.1. Low Reynolds number k–ε model

In the low Reynolds number formulation, the Eqs. (12), (14) and (15) are modified to incorporate the effect of the wall. The low Reynolds model correctly predicts the flow in the viscous layer, next to the wall. These modifications are usually implemented in such a way that model reduces to its standard form in the regions away from the wall. Several variations of low Reynolds model (for example Chien, 1982; Nagano and Tagawa, 1990; Rodi and Mansour, 1993) are available in the literature. The model implemented here was proposed by Abe et al. (1994) (hereafter referred to as AKN model). It should be noted that the implementation method would not be significantly different for other variations of the low Reynolds number model.

The AKN model is developed by multiplying constant C_μ in Eq. (16) by f_μ and multiplying $C_{2\varepsilon}$ in Eq. (15) by g_ε. The f_μ is defined as follows:

$$f_\mu \equiv \left\{1 - \exp\left(-\frac{y^*}{14}\right)\right\}^2 \left[1 + \frac{5}{R_t^{3/4}}\exp\left(1 - \frac{R_t}{200}\right)^2\right] \tag{17}$$

and g_ε is defined as

$$g_\varepsilon \equiv \left\{1 - \exp\left(-\frac{y^*}{3.1}\right)\right\}^2 \left[1 - 0.3\exp\left(1 - \frac{R_t}{6.5}\right)^2\right]. \tag{18}$$

In the above equations y^* is defined as follows:

$$y^* \equiv \frac{u_\varepsilon d}{\nu} \tag{19}$$

where d is the normal distance of the node center from the wall and $u_\varepsilon = (\nu\varepsilon)^{1/4}$. In Eqs. (17) and (18) R_t is defined as follows:

$$R_t \equiv \frac{k^2}{\nu\varepsilon}. \tag{20}$$

In addition to the boundary condition on the velocity components, boundary conditions for the k and ε are also needed. Since no slip and no penetration condition are applied at the walls, the k goes to zero at the walls. The boundary condition for ε, can be derived from Eq. (13). At the wall, k, ν_t and the velocity are zero. Moreover, derivatives of velocity in the direction parallel to the wall are also zero. Therefore, Eq. (13) reduces to the following:

$$\varepsilon_{\text{wall}} = \nu\frac{\partial^2 k}{\partial n^2} \tag{21}$$

where n is the wall normal direction. The above equation is used as the boundary condition for ε. The model constants for the AKN model are slightly different from the standard k–ε model and are given in Table 2.

4.2. High Reynolds number k–ε model

Although, the AKN model given above is in general valid for any Reynolds number, extremely fine grid is needed to resolve thin viscous layers formed in the case of high Reynolds number flows. For this reason it is often used only for low Reynolds number flows. To avoid increased computational load because of the need for a much finer grid, a different strategy is used for the high Reynolds number flows (Durbin and Reif, 2001).

It is well known that in flows parallel to a wall (flow over a flat plate, channel flow or pipe flow) there is a region where velocity follows log-law. In the channel and pipe flow the region lies between

Table 1
Values of model constants in the standard k–ε model.

$C_{1\varepsilon}$	$C_{2\varepsilon}$	C_μ	σ_ε	σ_k
1.44	1.92	0.09	1.2	1.0

Table 2
Values of model constants used in the AKN low Reynolds number model.

$C_{1\varepsilon}$	$C_{2\varepsilon}$	C_μ	σ_ε	σ_k
1.5	1.9	0.09	1.4	1.4

distances, $d^+ = 30$ and $d/\delta = 0.3$, from the wall, where δ is the half-width of the channel (or radius of the pipe), and the distance d^+ is in the wall units. A distance in the wall units is defined as

$$d^+ \equiv \frac{du_\tau}{\nu} \tag{22}$$

where μ_τ is defined as

$$u_\tau \equiv \sqrt{\frac{\tau_{\text{wall}}}{\rho}} \tag{23}$$

Here, τ_{wall} is the shear stress at the wall.

In the high Reynolds number model, it is assumed that the flow is predominantly parallel to the wall in its vicinity. The assumption can be considered valid in many cases because the flow is essentially parallel to the walls in the boundary layers. However, the validity of log-law cannot be assumed in the regions where flow is not parallel to one of the walls, as is the case for flow near the corner formed by any two walls. Nevertheless, the model is commonly used for all the flows because of its relative simplicity.

Two cells near a wall are shown in Fig. 1. In the high Reynolds number model, the cells near the wall are chosen in such a way that the interface shown in the figure lies in the log-law region. The standard k–ε equations are solved for all the cells except for the cells adjacent to the wall. At the interface shown in Fig. 1, the friction velocity (μ_τ) is evaluated from the following equation

$$\frac{U_1 - U_{\text{wall}}}{u_\tau} = \frac{1}{\kappa} \log y_1^+ + 5.5 \tag{24}$$

where, y_1^+ is the distance of the abovementioned interface from the wall in the wall units, $U_1 - U_{\text{wall}}$ is the speed of the fluid at that interface relative to the wall, and κ is the von Karman constant and has been assigned a value of 0.41. The k and ε equations are not solved in the cell next to wall. Instead, the following boundary conditions for these equations are applied at the interface shown in Fig. 1.

$$k = \frac{u^2}{\sqrt{C_\mu}} \tag{25}$$

$$\varepsilon = \frac{u^3}{n\sqrt{C_\mu}} \tag{26}$$

where n is the distance of the abovementioned interface from the wall. The reason for using these boundary conditions can be found in the standard text books on turbulence modeling (e.g. Durbin and Reif, 2001).

The U_1 in Eq. (24) is obtained by solving the momentum equation for the velocity component parallel to the wall. The flow in the near wall region is laminar and hence the convection terms are ignored during the solution of the equation. Also, the wall normal velocity is made zero at the interface discussed above. The cells on the edges between two surfaces need to be treated differently because there is one velocity component parallel to one of the wall and another component parallel to the other wall. Therefore, both of these velocity components need to be evaluated. The above method for solving for U_1, which is used in the present work, is given by Nonino and Giudice (1988). Alternatively, equation for U_1 can also be derived by using $\nu \partial U/\partial n = \tau_{\text{wall}}$ where n is wall normal direction and τ_{wall} can be obtained from Eq. (23) (Durbin and Reif, 2001).

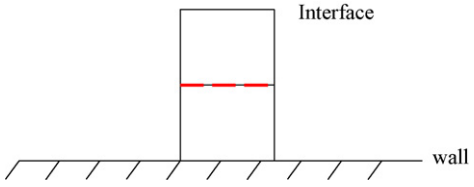

Fig. 1. Two cells next to the wall. The interface shown by the dashed (red) line should lie in the region where log-law is valid. (For interpretation of the references to color in this figure legend, the reader is referred to the web version of the article.)

5. Implementation of k–ε model using MNIM

In Section 2, the MNIM for the Navier–Stokes and convection–diffusion equation was discussed. Though, the scheme developed is valid for spatially varying dynamic viscosity (or diffusion coefficient), it has been previously developed only for constant properties. Since, the eddy viscosity is a variable quantity; the Navier–Stokes equation *in a cell* is approximated as follows:

$$\frac{\partial \bar{u}_m}{\partial t} + \bar{u}_p \frac{\partial \bar{u}_m}{\partial x_p} = -\frac{1}{\rho}\frac{\partial p}{\partial x_m} + (\nu + \nu_t)\frac{\partial^2 \bar{u}_m}{\partial x_p \partial x_p} + b_m \tag{27}$$

where, ν_{t0} in a cell at the current time step is defined in terms of the cell averaged k and ε, as follows:

$$\nu_{t0i,j,k,n} = C_\mu \frac{(\bar{k}^{xyz}_{i,j,k,n})^2}{\bar{\varepsilon}^{xyz}_{i,j,k,n}} \tag{28}$$

The above equation is obtained by writing Eq. (16) in terms of the discrete variables. Note that this value of the eddy viscosity is an approximation of the cell averaged eddy viscosity. In this approximation the average of products is approximated by the product of the averages. The approximation is second-order accurate as has been discussed previously.

Since, the diffusion coefficients (or the viscosity) for the equations solved is not constant in space. The diffusion coefficient in a cell is approximated by the average of the diffusion coefficient in that cell. Moreover, unlike the constant property case, the derivatives at the cell interfaces are not continuous; instead the product of diffusion coefficient and the derivative is continuous. The modified F coefficients (see Eqs. (4)–(7)) required for the Navier–Stokes, k and ε equations can be evaluated based on the diffusion coefficient in the respective equation and considering the modified equation for the continuity of flux. The f coefficient (see Eq. (9)), which is obtained by averaging the source term over the cell, remains the same for the Navier–Stokes equations.

Retaining the convection, diffusion and time derivative terms on the left hand side and treating all the other terms in the equations of k and ε as source terms, the development follows in the manner similar to that for the generic convection–diffusion equation discussed in Section 2. Since the diffusion coefficients for these equations also vary in space, they can hence be treated in the same way as discussed above for the Navier–Stokes equation. Obviously, the F coefficients for these equations are different from those for the Navier–Stokes equation and need to be evaluated separately for each of these equations. Considering the source terms, the f coefficient, which depend only on the source terms, needs to be evaluated for each of these equations.

The f coefficient for the ε equation (called f_ε) is evaluated as follows:

$$f_\varepsilon = 2C_{1\varepsilon}\frac{\varepsilon_0}{k_0}\nu_{t0}(\bar{s}_{mp}\bar{s}_{mp})_0 - C_{2\varepsilon}\frac{\varepsilon_0^2}{k_0} \tag{29}$$

Ideally, the k_0 and ε_0 for a cell in the above equation should be obtained by averaging k and ε, respectively, over space and time in that cell. However, since in the present work only steady-state solution is considered, the quantities averaged only over space are used instead (e.g. $\varepsilon_{0i,j,k,n} \approx \bar{\varepsilon}^{xyz}$). This may results in *false transients*; however, the steady-state solutions will not be affected. The product of various derivatives of velocities with respect to x, y and z appear in the equation for $\bar{s}_{mp}\bar{s}_{mp}$. The $(\bar{s}_{mp}\bar{s}_{mp})_0$ is the time-space average of $\bar{s}_{mp}\bar{s}_{mp}$ over a cell and can be evaluated in the same fashion as other

terms of similar type are evaluated by approximating average of the products by the product of the averages. It should be noted that the average of products is approximated again by product of averages in the evaluation of f_ε.

Similarly, f_k is obtained as follows:

$$f_k = 2\nu_{t0}(\bar{s}_{mp}\bar{s}_{mp})_0 - \varepsilon_0 \tag{30}$$

Values on the right hand side of Eq. (30) are evaluated in the same way as in Eq. (29).

Details of the implementation of the low Reynolds number and high Reynolds number models in the MNIM code are discussed in the next two sub-sections.

5.1. Implementation of low Reynolds number k–ε model using MNIM

The f_μ and g_ε (which involve k and ε) are evaluated by replacing k and ε by $\bar{k}^{xyz}_{i,j,k,n}$ and $\bar{\varepsilon}^{xyz}_{i,j,k,n}$, respectively. The distance d in Eq. (17) is considered to be the distance of the cell center from the wall.

One problem commonly found in low Reynolds number models is that values of k and/or ε can become negative during the false transients (or during iterations) which commonly leads to iterations that do not converge. To overcome this problem, the discretized equation corresponding to the k equation (Eq. (12)) needs to be modified. The above-mentioned discretized equation (see Eq. (8)) is given as

$$\begin{aligned} &F_{77}\bar{k}^{xyz}_{i,j,k,n} - F_{78}\bar{k}^{xyz}_{i,j,k,n-1} \\ &= 2\nu_{t0}\left(\bar{s}_{mp}\bar{s}_{mp}\right)_0 - \bar{\varepsilon}^{xyz}_{i,j,k,n}\frac{\bar{k}^{xyz}_{i,j,k,n}}{\bar{k}^{xyz}_{i,j,k,n-1}} + F_{71}\bar{k}^{xyt}_{i,j,k,n} + F_{72}\bar{k}^{xyt}_{i,j,k-1,n} \\ &\quad + F_{73}\bar{k}^{yzt}_{i,j,k,n} + F_{74}\bar{k}^{yzt}_{i-1,j,k,n} + F_{75}\bar{k}^{zxt}_{i,j,k,n} + F_{76}\bar{k}^{zxt}_{i,j-1,k,n}. \end{aligned} \tag{31}$$

In the above equation, source term (f_k) is used from Eq. (30). However, it is modified by multiplying the cell averaged k at the current time step and dividing by the similarly averaged k at the previous time step. Eq. (31) can now be written as follows:

$$\begin{aligned} &\left(F_{77} + \frac{\bar{\varepsilon}^{xyz}_{i,j,k,n}}{\bar{k}^{xyz}_{i,j,k,n-1}}\right)\bar{k}^{xyz}_{i,j,k,n} - F_{78}\bar{k}^{xyz}_{i,j,k,n-1} \\ &= 2\nu_{t0}\left(\bar{s}_{mp}\bar{s}_{mp}\right)_0 + F_{71}\bar{k}^{xyt}_{i,j,k,n} + F_{72}\bar{k}^{xyt}_{i,j,k-1,n} + F_{73}\bar{k}^{yzt}_{i,j,k,n} \\ &\quad + F_{74}\bar{k}^{yzt}_{i-1,j,k,n} + F_{75}\bar{k}^{zxt}_{i,j,k,n} + F_{76}\bar{k}^{zxt}_{i,j-1,k,n}. \end{aligned} \tag{32}$$

The advantage of using this formulation is that the source term in the above equation, $2\nu_{t0}(\bar{s}_{mp}\bar{s}_{mp})_0$, is always positive during the transients. This precludes the possibility of negative values of k during the transient. Similar modification in ε equation results in the following discretized equation:

$$\begin{aligned} &\left(F_{77} + g_\varepsilon C_{2\varepsilon}\frac{\bar{\varepsilon}^{xyz}_{i,j,k,n-1}}{\bar{k}^{xyz}_{i,j,k,n-1}}\right)\bar{\varepsilon}^{xyz}_{i,j,k,n} - F_{78}\bar{\varepsilon}^{xyz}_{i,j,k,n-1} \\ &= 2C_{1\varepsilon}\frac{\bar{\varepsilon}^{xyz}_{i,j,k,n-1}}{\bar{k}^{xyz}_{i,j,k,n-1}}\nu_{t0}(\bar{s}_{mp}\bar{s}_{mp})_0 + F_{71}\bar{\varepsilon}^{xyt}_{i,j,k,n} + F_{72}\bar{k}^{xyt}_{i,j,k-1,n} \\ &\quad + F_{73}\bar{\varepsilon}^{yzt}_{i,j,k,n} + F_{74}\bar{\varepsilon}^{yzt}_{i-1,j,k,n} + F_{75}\bar{\varepsilon}^{zxt}_{i,j,k,n} + F_{76}\bar{\varepsilon}^{zxt}_{i,j-1,k,n} \end{aligned} \tag{33}$$

Similarly, to prevent ε becoming negative during the transient, the boundary condition (Eq. (21)) is approximated as follows:

$$\varepsilon_{\text{wall}} = 2\nu\frac{k_1}{n_1^2} \quad \text{or} \quad \varepsilon_{\text{wall}} = 2\nu\frac{\partial\sqrt{k}}{\partial n^2} \tag{34}$$

where k_1 and n_1 are the turbulence kinetic energy and the distance from the wall of the interface of the first and second cells in the wall normal direction, respectively. In the present work, first of the two boundary conditions is used. For a wall parallel to the y–z plane the ε boundary condition is implemented as follows:

$$\bar{\varepsilon}^{yzt}_{i-1,j,k} = 2\nu\frac{\bar{k}^{yzt}_{i,j,k}}{2a_i}. \tag{35}$$

Here, the left surface of the (i, j, k) cell is assumed to be on the wall. The boundary conditions for walls in the other directions can be similarly implemented.

5.2. Implementation of high Reynolds number k–ε model using MNIM

The momentum equation for the velocity component parallel to the wall in the cells next to the walls has to be solved without the convection terms. This can be implemented by modifying the F coefficients and f term in that particular cell. For the case in which u-component of the velocity is parallel to the wall, this can be achieved by forcing u_p and u_0 to be zero in that cell (see Eqs. (10) and (11)). Implementation is similar for the walls parallel to the other directions.

For the flow in the x-direction near a wall parallel to the x–z plane, Eq. (24) is written as follows:

$$\frac{\bar{u}^{zxt}_{i,j,k} - \bar{u}^{zxt}_{i,j-1,k}}{u_\tau} = \frac{1}{\kappa}\log\frac{2b_j\nu}{u_\tau} + 5.5 \tag{36}$$

In the above equation wall is located at the surface indexed by (i, $j-1$, k).

Here, the left surface of the (i, j, k) cell is assumed to be on the wall. Similar equations can be written for walls parallel to any other direction. The above equation is a non-linear equation to be solved for u_τ. The Newton–Raphson iteration scheme is used to solve this equation. Following function is defined for the Newton iterations:

$$G(u_\tau) = \frac{\bar{u}^{zxt}_{i,j,k} - \bar{u}^{zxt}_{i,j-1,k}}{u_\tau} - \frac{1}{\kappa}\log\frac{2b_j\nu}{u_\tau} + 5.5 \tag{37}$$

and the iterations are then implemented as follows:

$$u^{m+1} = u^m - \frac{G(u^m)}{G'(u^m)} \tag{38}$$

where, m is the iteration number and $G'(u_\tau)$ is the derivative of the function $G(u_\tau)$ with respect to u_τ. The iterations are performed till $G(u_\tau)$ is reasonably small (less than a pre-specified limit). Though, subscript (i, j, k) are not used for u_τ, it should be noted that it needs to be evaluated for each cell next to the wall. Once u_τ is evaluated, the implementation of the boundary conditions for the k and ε equations is straightforward.

6. Results for low Reynolds number model

The MNIM implementation of the k–ε model is tested using the fully developed channel flow. Although the problem is one-dimensional, it is a good test case because the low Reynolds number k–ε models are generally calibrated using this problem so as to match the channel flow characteristics. Therefore, successful implementation of the k–ε model using MNIM should be able to produce good match with DNS results (or with experimental) data. The scheme is implemented on 2D version of MNIM with periodic boundary conditions for the velocity, k and ε in the streamwise direction. A constant pressure gradient is applied at the inlet of the channel and a constant pressure is maintained at the outlet. The results are presented here for two Reynolds number

s: $Re_\tau = 180$ and $Re_\tau = 550$. The Re_τ is friction Reynolds number and is defined as follows for the channel flow:

$$Re_\tau = \frac{\nu u_\tau}{\delta}. \quad (39)$$

The results are compared with the DNS results available at the website (http://torroja.dmt.upm.es/ftp/channels/data/) mentioned by del Alamo and Jimenez (2003).

6.1. Channel flow with $Re_\tau = 180$

The velocity, turbulent kinetic energy and dissipation rate plots are given in Fig. 2(a)–(c), respectively. The DNS results are also plotted for comparison. Two different non-uniform grids are used for the solution of this problem. The first grid has 6 cells in the wall normal direction and the successive ratio of the length of the cells in the wall normal direction is 1.7. Second grid has 10 cells in the wall normal direction and abovementioned successive ratio is 1.1.

6.2. Channel flow with $Re_\tau = 550$

The same number of cells are used for the simulation of the flow with $Re_\tau = 550$ as that for the $Re_\tau = 180$. However, because of the thinner boundary layers the grids used are more non-uniform. The successive grids with 10 cells in the wall normal direction have a ratio of 1.2 and that with 6 cells have a ratio of 1.8. Fig. 3(a)–(c) show the velocity, k and ε, respectively, for this Reynolds number case.

Overall, the results compare very well with the DNS results for the velocities for both Reynolds numbers. The ε values near the wall show a peak, which is different from the behavior observed in the DNS results. However, the AKN model is known to show this discrepancy in the ε values (Park and Sung, 1994). The discrepancy in the k values is similar to that seen in the original implementation of the AKN model by Abe et al. (1994) and is not due to any deficiency in the MNIM.

Since low Reynolds number model are constructed so as to match the behavior of the flow in the viscous layer near the wall, it is necessary to have grid points inside the thin viscous layer for the low Reynolds number model. This also explains the fact that very coarse grid away from the wall also show good agreement with DNS results as long as the near wall region is resolved reasonably well. Therefore, near wall grid resolution required, in general, is independent of the numerical scheme used to implement the model.

7. Results for high Reynolds number model

7.1. Channel flow with $Re_\tau = 2000$

The channel flow with relatively high Reynolds number i.e. $Re_\tau = 2000$ is used for testing the high Reynolds number model. For the high Reynolds number model, u_τ is computed using Eq. (36). The equations are solved over the entire channel, and the boundary conditions are applied as discussed previously for the high Reynolds number model. First two grids used for this case are uniform with 10 and 20 cells in the wall normal direction. Third grid used is a non-uniform grid with only 10 cells in the wall normal direction. The ratio between the dimensions of the successive cells in the wall normal direction is 1.1. Non-uniform grids are used making sure that the interface in Fig. 1 lies in the log-law region. The results are shown in the Fig. 4(a), (b) and (c) for velocity, k and ε, respectively. The non-uniform 10 cell grid results are as good as 20 cell grid. Both these results match very well with the DNS results except for some discrepancy in k values. The DNS results used here are stored

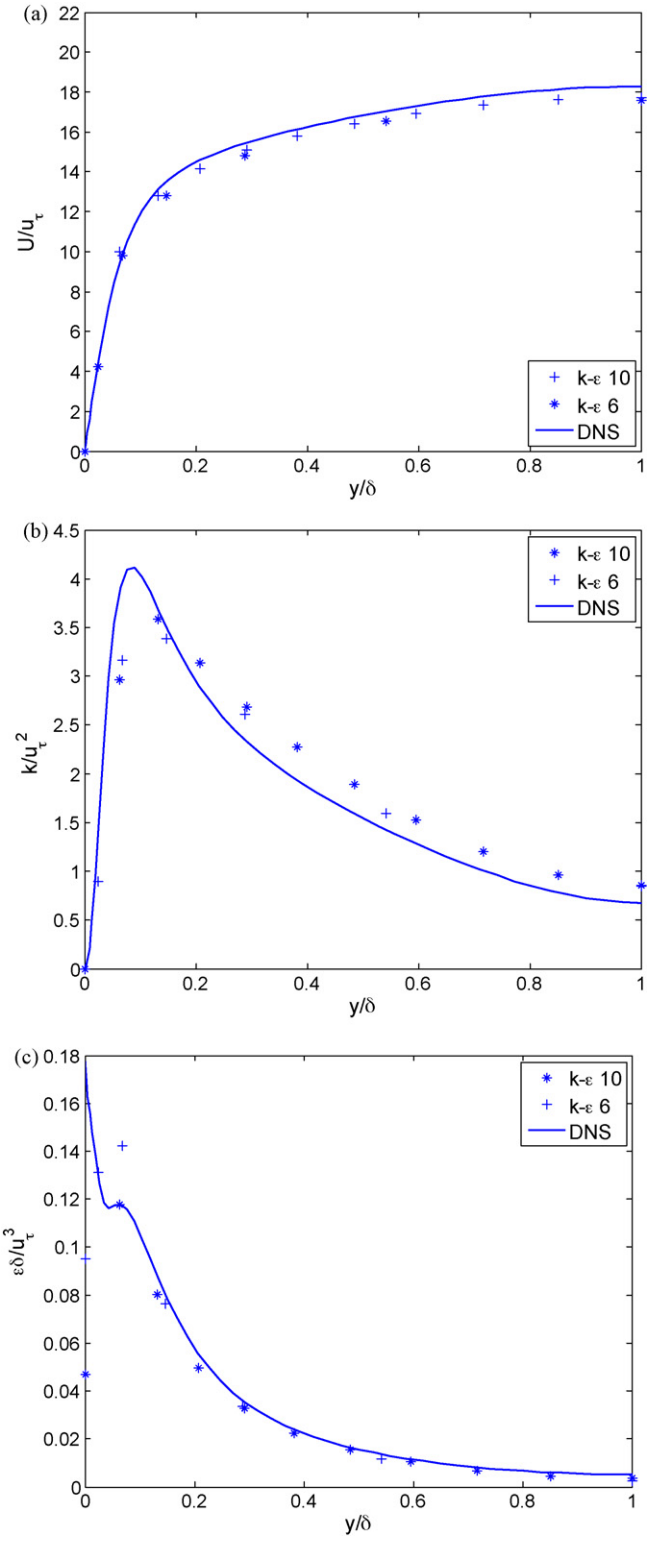

Fig. 2. The comparison of (a) axial velocity; (b) turbulent kinetic energy and; (c) dissipation of turbulent kinetic energy obtained using the low Reynolds number k–ε model and the DNS results (for $Re_\tau = 180$).

at the website (http://torroja.dmt.upm.es/ftp/channels/data/) cited by Hoyas and Jimenez (2006).

7.2. Lid driven cavity with $Re = 20{,}000$

The high Reynolds number model is used to solve the lid driven cavity problem. A non-uniform 30×30 grid is used for the

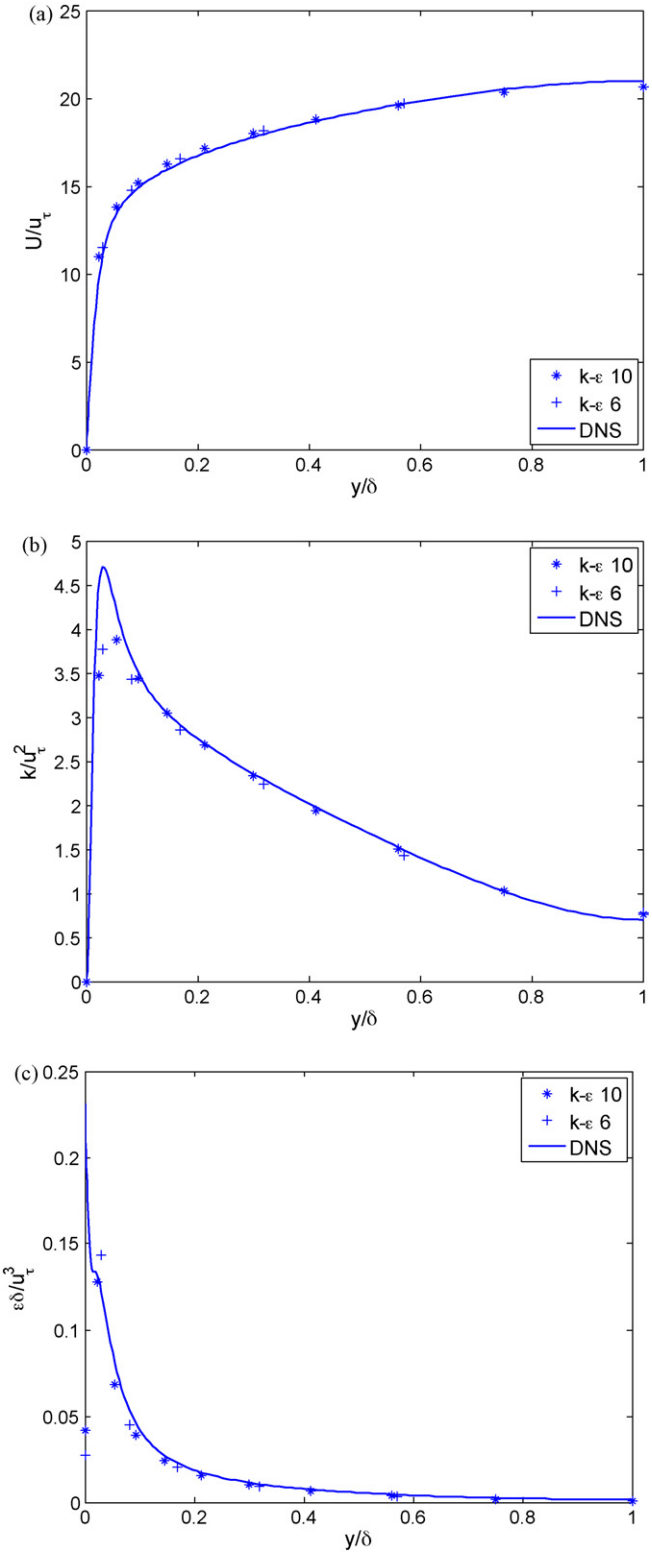

Fig. 3. The comparison of (a) axial velocity; (b) turbulent kinetic energy and; (c) dissipation of turbulent kinetic energy obtained using the low Reynolds number k–ε model and the DNS results (for $Re_\tau = 550$).

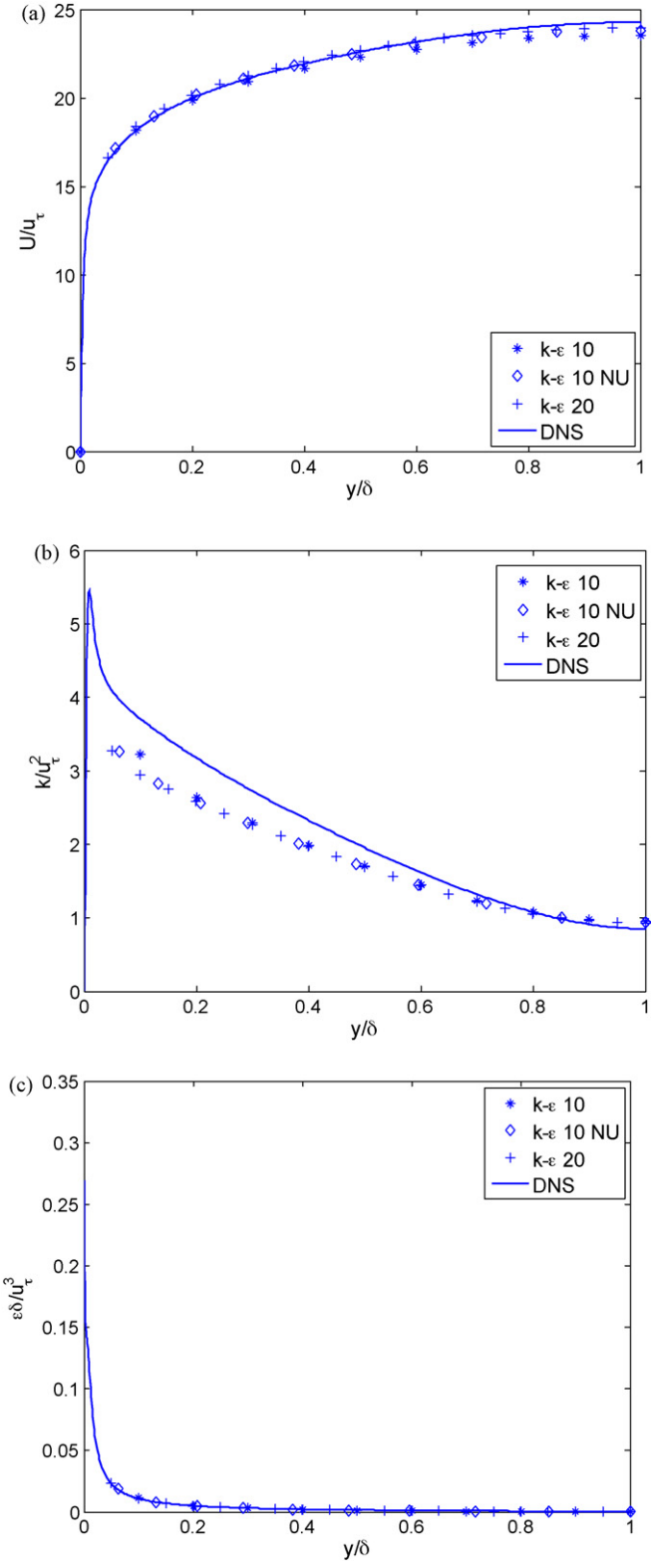

Fig. 4. The comparison of (a) axial velocity; (b) turbulent kinetic energy and; (c) dissipation of turbulent kinetic energy obtained using the high Reynolds number k–ε model and the DNS results (for $Re_\tau = 2000$).

simulation. The plot of the u-component of the velocity at the vertical mid-plane and the v-component of the velocity at the horizontal mid-plane are shown in Figs. 5(a) and 6(b), respectively. Figs. 5(b) and 6(b) show the plots of DNS results for similar3D cubic cavity for $Re = 12{,}000$. These latter figures are taken from Bouffanais et al. (2007) who carried out LES simulations of the lid driven cavity problem. The DNS results shown in those figures are from Leriche and Gavrilakis (2000). The DNS results at $Re = 12{,}000$ are shown because the results for higher Re are not available. The

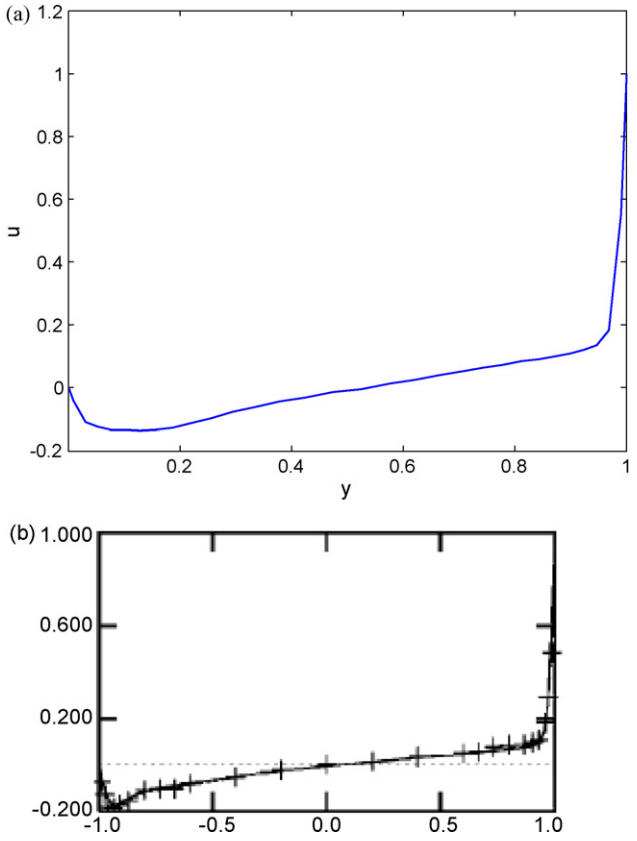

Fig. 5. Plot of u-velocity for lid driven cavity at the vertical mid-plane. (a) Obtained using the high Reynolds number k–ε model (b) obtained using the DNS (solid line) approach (taken from Bouffanais et al., 2007).

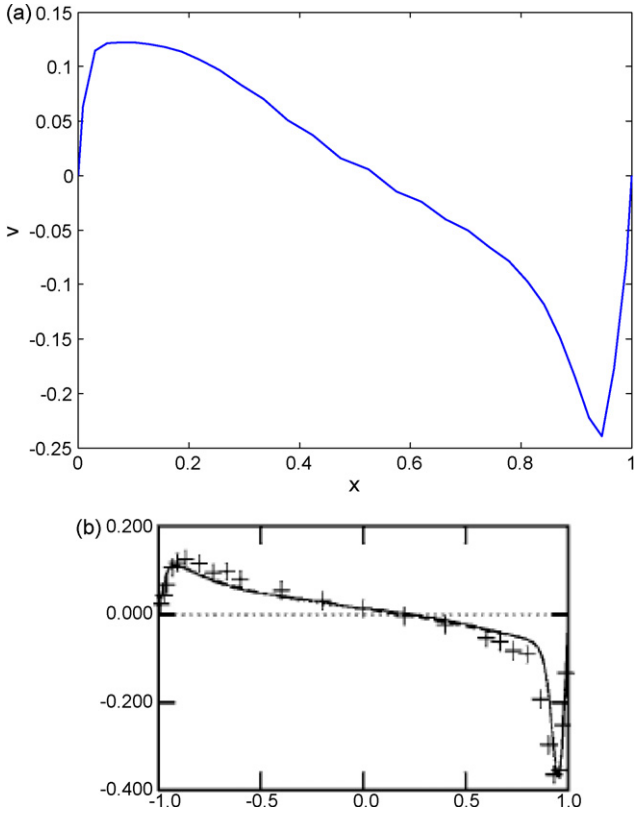

Fig. 6. Plot of v-velocity for lid driven cavity at the horizontal mid-plane. (a) Obtained using the high Reynolds number k–ε model; (b) obtained using the DNS (solid line) approach (taken from Bouffanais et al., 2007).

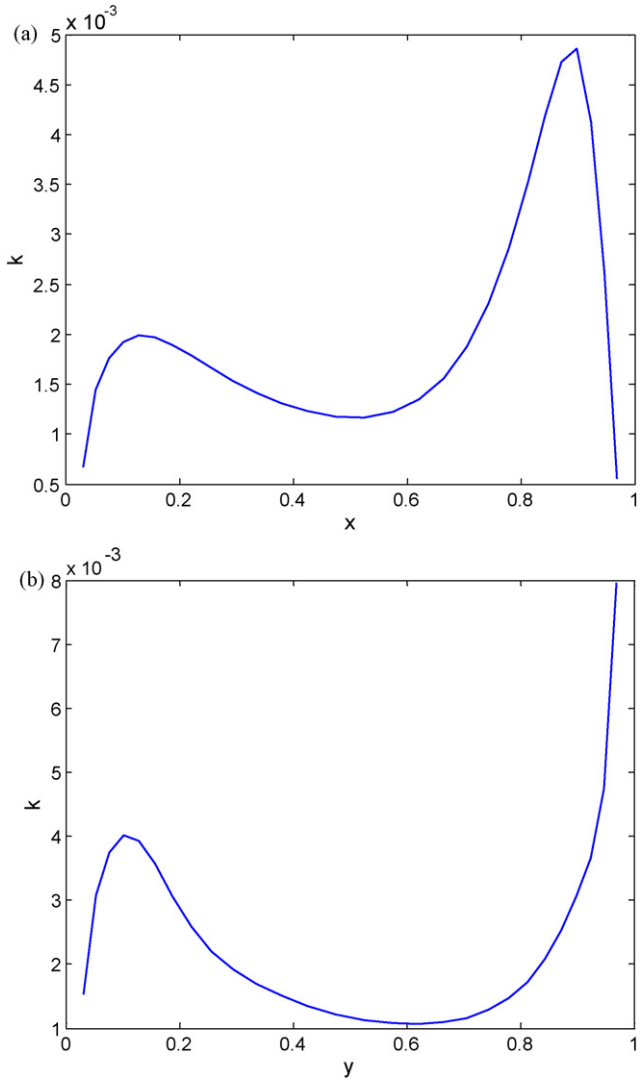

Fig. 7. Plot of k for the lid driven cavity at (a) the vertical mid-plane and (b) at the horizontal mid-plane obtained using the high Reynolds number k–ε model.

k–ε model is not used to simulate the flow for $Re = 12{,}000$ because at this Re the flow in most of the domain is laminar (Leriche and Gavrilakis, 2000). In addition to the plots of the velocity, the k at the vertical mid-plane is plotted in Fig. 7(a) and that at the horizontal mid-plane is shown in Fig. 7(b). The corresponding ε plots are shown in Fig. 8(a) and (b), respectively. The DNS results for the k and ε values are not available. However, the plots for these values are qualitatively similar to the plots given by (Nonino and Giudice, 1988) (not shown here). The direct comparison is not possible because of very coarse grid used in the abovementioned reference.

It can be seen from the plots of velocity, although the values of the velocity are significantly different, DNS and k–ε model have qualitatively similar results. The significant differences in these results are, however, expected because of various assumptions made in the k–ε model. Also, the spatial variation of k matches qualitatively with the results reported by Nonino and Giudice (1988) (not shown here). Direct comparison with those results is not possible because of very coarse grid used in the reference mentioned above.

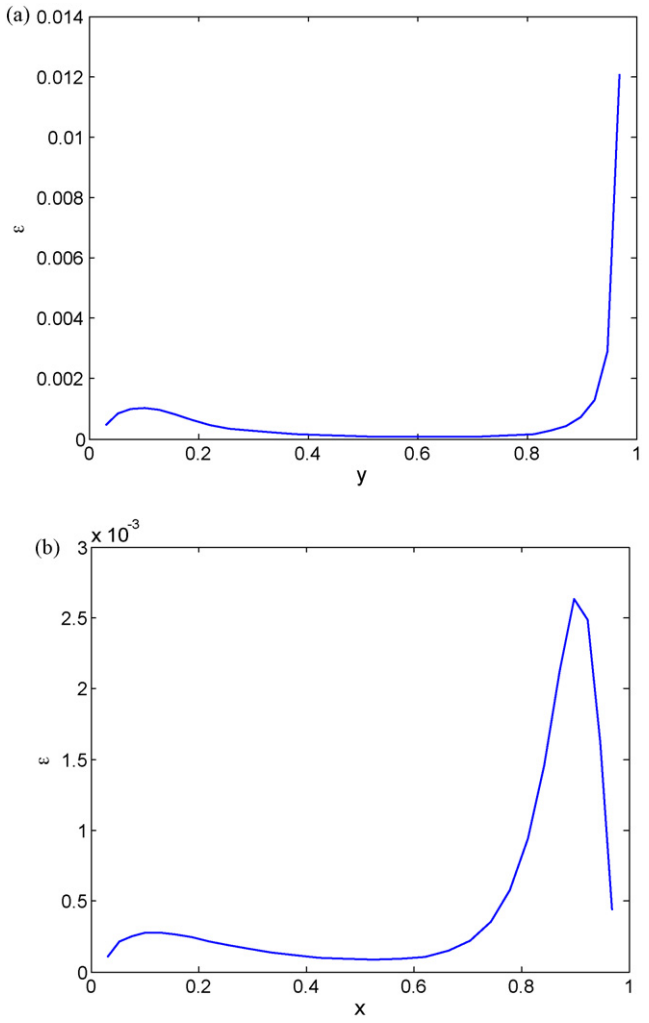

Fig. 8. Plot of ε for the lid driven cavity at (a) the vertical mid-plane and (b) at the horizontal mid-plane obtained using the high Reynolds number k–ε model.

8. Conclusions

The implementation of the k–ε model using the MNIM formulation is discussed in the present work. This implementation has been carried out for two variations of the model, one based on high Reynolds number approach and another based on the low numbers approach. The other variations of these models can be implemented in a similar manner as underlying features of these models are quite similar. The results obtained by using the developed numerical scheme are compared with the DNS results from various sources in the literature. In general, the discrepancies seen in the present work are same as those reported for the simulations carried out using other numerical schemes. From the abovementioned observation it can be inferred that the difference between the DNS results and current implementation arises mainly from the assumptions made in the k–ε model and hence is due to the limitations of the k–ε model rather than the choice of the numerical scheme in the present work.

It is seen that very coarse grids can be used away from the walls for the present simulation. This is especially true for low Reynolds number model. In the high Reynolds number case, the near wall grid resolution is restrained by the fact that the interface between the first and second cell must lie on the log-law region. Similarly, in the low Reynolds number model, the resolution of the near wall viscous layer is necessary. Therefore, near wall grid refinement is more dependent on the k–ε model used, than on the choice of the numerical scheme used for the simulation. However, away from the wall relatively few cells are needed.

References

Abe, K., Kondoh, T., Nagano, Y., 1994. A new turbulence model for predicting fluid flow and heat transfer in separating and reattaching flows—I. Flow field calculations. Int. J. Heat Mass Transfer 37, 139–151.

Azmy, Y.Y., Dorning, J.J., 1983. A nodal integral approach to the numerical solution of partial differential equations. Adv. React. Comput. II, 893–909.

Azmy, Y.Y., 1985. Nodal method for problems in fluid mechanics and neutron transport, Ph.D. thesis, University of Illinois.

Bouffanais, R., Deville, M.O., Leriche, E., 2007. Large-eddy simulation of the flow in a lid-driven cubical cavity. Phys. Fluids 19, 055108.

Chien, K.Y., 1982. Predictions of channel and boundary-layer flows with a low Reynolds number turbulence model. AIAA J. 20, 33–38.

del Alamo, J.C., Jimenez, J., 2003. Spectra of the very large anisotropic scales in turbulent channels. Phys. Fluids 15, L41–L44.

Durbin, P.A., Reif, B.A.P., 2001. Statistical Theory and Modeling for Turbulent Flows. John Wiley & Sons Ltd., New York.

Elnawawy, O.A., Valocchi, J., Ougouag, A.M., 1990. The cell analytical–numerical method for solution of the advection–dispersion equation: two-dimensional problems. Water. Resour. Res. 26, 2705–2716.

Esser, P.D., Witt, R.J., 1993. An upwind nodal integral method for incompressible fluid flow. Nucl. Sci. Eng. 114, 20–35.

Hennart, J.P., 1986. A general family of nodal schemes. SIAM J. Sci. Stat. Comp. 7, 264–287.

Horak, W.C., Dorning, J.J., 1985. A nodal coarse-mesh method for the efficient numerical solution of laminar flow problems. J. Comp. Phys. 59, 405–440.

Hoyas, S., Jimenez, J., 2006. Scaling of velocity fluctuations in turbulent channels up to $Re_\tau = 2000$. Phys. Fluids 18, 011702.

Lawrence, R.D., 1986. Progress in nodal methods for the solutions of the neutron diffusion and transport equations. Prog. Nucl. Energy 17, 271–301.

Leriche, E., Gavrilakis, S., 2000. Direct numerical simulation of the flow in the lid-driven cubical cavity. Phys. Fluids 12, 1363–1376.

Michael, E.P.E., Dorning, J.J., Rizwan-uddin, 2001. Studies on nodal integral methods for the convection–diffusion heat equation. Nucl. Sci. Eng. 137, 380–399.

Nagano, Y., Tagawa, M., 1990. An improved k–epsilon model for boundary layer flows. J. Fluids Eng. 112, 33–39.

Nonino, C., Giudice, S.D., 1988. Finite element analysis of turbulent forced convection in lid-driven rectangular cavities. Int. J. Numer. Meth. Eng. 25, 313–329.

Park, T.S., Sung, J., 1994. A nonlinear low-Reynolds-number model for turbulent separated and reattaching flows: flow field computations. Int. J. Heat Mass Transfer 38, 2657–2666.

Rodi, W.N., Mansour, N., 1993. Low Reynolds number k–epsilon modeling with the aid of direct simulation data. J. Fluid Mech. 250, 509–529.

Wang, F., Rizwan-uddin, 2003. A modified nodal scheme for the time-dependent, incompressible Navier–Stokes equations. J. Comp. Phys. 187, 168–196.

Wang, F., Rizwan-uddin, 2005. Modified nodal integral method for the three-dimensional time-dependent incompressible Navier–Stokes equations. Nucl. Sci. Eng. 149, 107–114.

Wescott, B., Rizwan-uddin, 2001. An efficient formulation of the modified nodal integral method and application to the two dimensional Burgers equation. Nucl. Sci. Eng. 139, 293–305.

Wilson, G.L., Rydin, R.A., Azmy, Y.Y., 1988. Time-dependent nodal integral method for the investigation of bifurcation and nonlinear phenomena in fluid flow and natural convection. Nucl. Sci. Eng. 100, 414–425.